THE JOURNAL OF PHYSICAL CHEMISTRY B

Article

pubs.acs.org/JPCB

Role of Red-Ox Cycle in Structural Oscillations and Solvation Dynamics in the Mitochondria of a Live Cell

Shyamtanu Chattoraj,[†] Rajdeep Chowdhury,[†] Sumit Kumar Dey,[‡] Siddhartha Sankar Jana,*[,‡] and Kankan Bhattacharyya*[,†]

[†]Department of Physical Chemistry and [‡]Department of Biological Chemistry, Indian Association For The Cultivation of Science, Jadavpur, Kolkata 700 032, India

ABSTRACT: Structural oscillations and solvation dynamics in the mitochondria of a live cell are studied by time-resolved microscopy using a covalent fluorescence probe. We compared the dynamics in a human breast cancer cell (MCF-7) with that in a normal breast cell MCF-10A. The probe, CPM (7-diethylamino-3-(4-maleimido-phenyl)-4-methylcoumarin), binds with the free thiol groups. In MCF-10A cell, CPM binds with the discrete mitochondria. In MCF-7, CPM labels the clustered mitochondria in the perinuclear region. Location of the CPM in the mitochondria is confirmed by colocalization with a mitochondria-tracker dye. The red-ox cycle in the mitochondria causes periodic fluctuation in the microenvironment in the discrete mitochondria. This is manifested in fluctuations in fluorescence intensity of CPM bound to mitochondria. The magnitude of oscillation is much less for CPM bound to the clustered mitochondria (in which the red-ox cycle is inefficient) in the cancer cell (MCF-7). In both of the cells (MCF-10A and MCF-7) CPM bound to thiol-containing proteins in mitochondria exhibits ultraslow response with average solvation time ($\langle\tau_s\rangle$) of 850 and 1400 ps in MCF-10A and MCF-7, respectively.

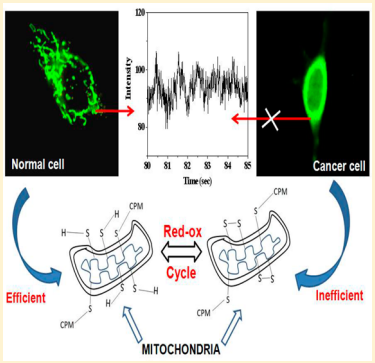

1. INTRODUCTION

One of the longstanding goals of ultrafast spectroscopy is to understand the dynamics in different locations in a living system (e.g., in different organelles inside a living cell). In recent years, there have been extensive applications of large-scale computer simulations[1−6] and ultrafast spectroscopy[7−15] to study dynamics in confined systems (in particular, of water molecules). The computer simulations provide high spatio-temporal resolution to describe dynamics in different molecular layers around a biomolecule.[1−6] The ultrafast experiments provide high temporal resolution with little or no spatial resolution. Confocal microscopy provides very high spatial resolution. As a result, single-molecule spectroscopy (confocal microscopy) has been applied to investigate interactions of many biological macromolecules. Xie and coworkers studied motion of transcription factor[16] and DNA repair enzyme[17,18] along a DNA. Lu and coworkers investigated intermittent coherent oscillations and fluctuation in donor−acceptor distances in an enzyme substrate complex.[19−22] Most recently, we have detected stochastic resonance in silencing of a gene in a live cell by short interfering RNA.[23] Single-molecule fluorescence spectroscopy has been employed to investigate structural organization and conformational changes of Kinesin-1 in live cells,[24] nucleotide binding to kinesin motor heads using fluorescent ATP analogue,[25] and dynamics of kinesin motor domain.[26] Surrey and coworkers investigated the dynamics of microtubule plus end-tracking protein using time-resolved microscopy.[27,28]

The living systems often exhibit oscillations or rhythms that control biological function through spatial and temporal organization.[29,30] The time periods of such oscillations vary from days (circadian rhythm) to seconds (e.g., beating motion of heart[31] or human airway muscle cell[32]) or milliseconds (fluctuations in membrane potential in various cells,[33−35] glycolytic oscillations,[36] and stochastic resonance[23,30]).

Many such oscillations are related to the intermittent structural changes associated with red-ox signaling pathways. For instance, at the surface of a cell exofacial thiols undergo repeated oxidation by the extracellular oxidants to disulfides, and the disulfides are reduced to thiols in the reducing intracellular environment.[37] Very recently, we have detected intermittent structural oscillation arising from the red-ox cycle in the membrane region of a live cell using a covalent probe (7-diethylamino-3-(4-maleimido-phenyl)-4-methylcoumarin, CPM).[38]

Similar red-ox cycles also occur in the mitochondria region of a cell.[39−58] The dynamics of mitochondrial thiol proteins is inherently related to the production of reactive oxygen species (ROS), which acts as a red-ox signaling molecule in the eukaryotic cell.[51] The ability of mitochondrial network to act as a biological oscillator has attracted vigorous recent attention. The oscillatory behavior of mitochondrial network is a collective consequence of different ROS generation rates,[45,51] fluctuation in inner mitochondrial membrane potential,[42−44] different thiol−disulfide exchange rates of mitochondrial thiol

Special Issue: Branka M. Ladanyi Festschrift

Received: April 18, 2014
Revised: May 8, 2014

   dx.doi.org/10.1021/jp503808z | J. Phys. Chem. B XXXX, XXX, XXX−XXX

proteins,[41,51] as well as Ca^{2+}regulation of mitochondrial ATP production.[50]

In this work, we show that the red-ox cycle in the mitochondria gives rise to structural oscillations. To demonstrate this, we have labeled the mitochondrial thiol proteins in two different cells (MCF-10A and MCF-7) using CPM as a covalent probe. Thus, we report, for the first time, on the structural oscillations and solvation dynamics in the mitochondria of a live cell.

2. EXPERIMENTAL SECTION

2.1. Materials. Laser-grade dye, CPM, and dimethyl sulfoxide (DMSO, Sigma, biological grade for cell culture) were used.

2.2. Methods. *2.2.1. Cell Preparation.* The MCF-7 (human nonmetastasis breast cell line) and the MCF-10A (human normal breast cell line) were purchased from the American Type Culture Collection (Manassas, VA). MCF-7 cells were cultured in DMEM (Dulbecco's modified Eagle medium) (Invitrogen) high glucose medium supplemented with 10% fetal bovine serum (FBS), 1% penicillin streptomycin glutamine, and 10 μg/mL insulin (Sigma), whereas MCF-10A cells were maintained in MEGM (mammary epithelial growth medium) with BulletKit supplements (Lonza) and 100 ng/mL cholera toxin (Sigma) at 37 °C with 5% CO_2. 2×10^3 cells were seeded on 30 mm confocal Petri dish and after 24 h of seeding it was incubated for 60 min with CPM dye solution (in DMSO) in phenol-red- and FBS-free DMEM medium to a final extracellular concentration of 100 nM. To minimize autofluorescence, we used a phenol-red-free culture (DMEM) medium. After rinsing the cells with phosphate-buffered saline (PBS) buffer solution, cells were used for microscopic study within 10 min. All experiments were carried out in ~25 °C. All experiments were repeated at least three times.

2.2.2. Experimental Setup for One Photon Microscopy. The experimental setup for one photon microscopy has been described in our previous publication.[59,60] In brief, a combination of confocal microscope (Olympus IX-71) and TCSPC setup (PicoQuant, MicroTime 200, numerical aperture (NA) ~1.2) and a pulsed picosecond diode laser (PDL 828-S "SEPIA II," Pico Quant, at 405 nm) were used. Thus, the diffraction limited spot size is $0.6\lambda/1.2 \approx \lambda/2$. For live-cell studies, we kept laser power at or below ~0.27 μW. Fluorescence with different polarizations ($I_{\parallel}$, and $I_{\perp}$) was separated using a polarizer cube (Chroma) and detected by two separate detectors (microphoton device, MPD). Appropriate narrow band-pass filters were used (e.g., XBPA480, 540, etc. Asahi Spectra) to collect TCSPC decay at specific emission wavelengths. The fluorescence lifetime decays under magic-angle conditions are as follows

$$I_{\text{magic}}(t) = I_{\text{II}}(t)\cos^2(54.75^\circ) + I_{\perp}(t)\cdot G\cdot\sin^2(54.75^\circ) = (1/3)I_{\text{II}}(t) + (2/3)\cdot G\cdot I_{\perp}(t) \quad (1)$$

G factor for this microscope setup was measured by tail fitting of fluorescein[61] and was found to be ~1.3. Fisz et al.[62] carried out a detailed analysis for one photon excitation fluorescence polarization microscopy under high-aperture excitation or detection.

Because the CPM dye covalently bonded to the thiol-containing proteins in the cell does not diffuse, we could not record the autocorrelation trace using fluorescence correlation spectroscopy (FCS). As a result, we do not know the value of $G(0)$, which gives the exact number of dye molecules (N) in the focal volume. To estimate N, we first obtained the focal volume as follows. The structure parameter (ω) of the focal volume is given by

$$\omega = \omega_z/\omega_{xy} \quad (2)$$

where ω_z and ω_{xy} are the longitudinal and transverse radii of the focal volume, respectively. From the reported diffusion coefficient of Rhodamine 6G in water (426 $\mu m^2\ s^{-1}$),[63] we obtained $\omega_{xy} \approx 319$ nm and $\omega \approx 5$. This corresponds to a focal volume 0.9 fL. From this value of focal volume, we estimate that the number of dye molecules (N) in the focal volume for a 100 nM dye solution is ~50.

Emission Spectra. The emission spectra of CPM in MCF-10A and MCF-7 cell were recorded using an electron multiplying charge-coupled device (EMCCD, ANDOR Technology) attached to a spectrograph (ANDOR Technology, Shamrock series).[59,60] We have used a dichroic mirror (Z405RDC, Chroma) and a suitable filter (HQ430lp, Chroma) to block the excitation laser light (405 nm). This causes slight distortion at the blue edge of the emission spectra.

Fluorescence Lifetime Measurement. For recording instrument response function (IRF), we used a bare slide and collected the scattered laser light. The FWHM of the IRF for excitation at 470 nm is ~100 ps. The fluorescence decay is deconvoluted using the IRF and DAS6 v6.3 software.

Solvation Dynamics under a Microscope. The time-resolved emission spectra (TRES) were constructed using the parameters of best fit to the fluorescence decays and the steady-state emission spectrum following the procedure described by Maroncelli and Fleming.[64]

The solvation dynamics is described by decrease in emission energy (frequency, ν) with increase in time. If $\nu(0)$, $\nu(t)$, and $\nu(\infty)$ are the emission frequencies at time 0, t, and ∞, respectively, the decreases in emission energy with time are described by

$$\nu(t) = \nu(\infty) + [\nu(0) - \nu(\infty)]\sum_i a_i e^{-t/\tau_i} \quad (3)$$

The time constants for solvation (τ_i) are obtained from the fitting of $\nu(t)$ versus t curves using eq 3. The other parameters, $\nu(0)$ and $\nu(\infty)$, are also obtained from this fitting.

The solvent correlation function, $C(t)$, can be defined as

$$C(t) = \frac{\nu(t) - \nu(\infty)}{\nu(0) - \nu(\infty)} \quad (4)$$

The solvent correlation functions $C(t)$ were fitted to a double-exponential decay as follows

$$C(t) = \sum_{i=1}^{2} a_i \exp(-t/\tau_i) \quad (5)$$

In our setup with IRF ~100 ps, we have obviously missed the ultrafast component of solvation dynamics, which occurs on the <100 ps time scale. The amount of solvation missed may be estimated using the Fee–Maroncelli procedure.[65] According to this procedure, theoretical emission frequency at $t = 0$ ($\upsilon_{\text{em}}^{\text{theo}}(0)$) is given by

$$\upsilon_{\text{em}}^{\text{theo}}(0) = \upsilon_{\text{abs}}^{\text{p}} - (\upsilon_{\text{abs}}^{\text{np}} - \upsilon_{\text{em}}^{\text{np}}) \quad (6)$$

dx.doi.org/10.1021/jp503808z | J. Phys. Chem. B XXXX, XXX, XXX–XXX

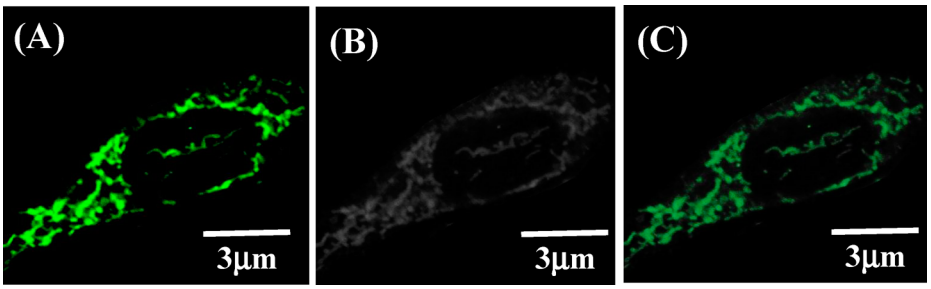

Figure 1. Confocal image of MCF-10A labeled with CPM: (A) fluorescence image, (b) gray-scale image, and (c) merged image.

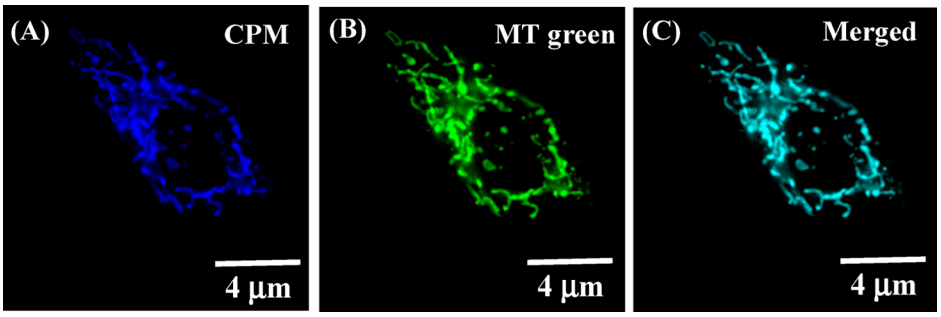

Figure 2. Confocal image of MCF-10A: (A) labeled with CPM, (B) labeled with MT-green, and (C) merged image.

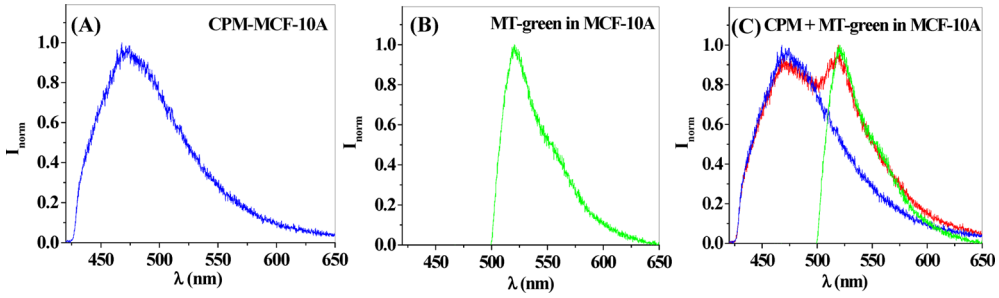

Figure 3. Emission spectra inside a MCF-10A: (A) CPM (blue), (B) MT-green (green), and (C) CPM and MT-green both (red).

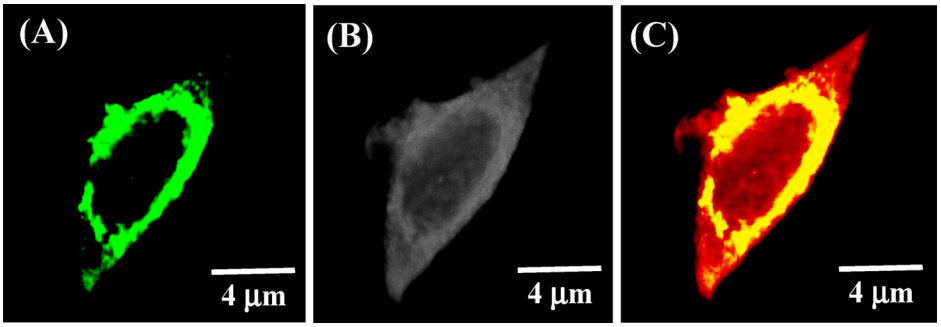

Figure 4. Confocal image of MCF-7 labeled with CPM: (A) fluorescence image, (B) gray-scale image, and (C) merged image (gray-scale image marked red to show contrast with CPM emission (yellow)).

υ_{abs}^{p} and υ_{abs}^{np} are absorption frequencies in polar (system) and nonpolar medium, respectively. υ_{em}^{np} denotes the emission frequency in nonpolar medium. It is not possible to record the absorption spectrum of a few molecules of the probe under a confocal microscope setup. Therefore, we have assumed the $\upsilon_{em}^{theo}(0)$ value of our system (CPM in live cell) to be the same as that in a bulk medium in which the emission maximum of CPM is the same as that in the live cell.[66]

3. RESULTS

3.1. Confocal Image. *3.1.1. Localization of CPM in Mitochondria of MCF-10A.* Figure 1 shows the confocal image of a single live breast cell MCF-10A stained by CPM. From the image (Figure 1A–C), it is clearly seen that CPM dye (~100 nM) localizes in the mitochondria of MCF-10A cell. CPM dye shows fluorescence only when it is covalently attached to a free thiol group of a protein.[66] Thus, the images (Figure 1) indicates that CPM dye is covalently bound to the mitochondrial thiol proteins, in MCF-10A.

dx.doi.org/10.1021/jp503808z | J. Phys. Chem. B XXXX, XXX, XXX–XXX

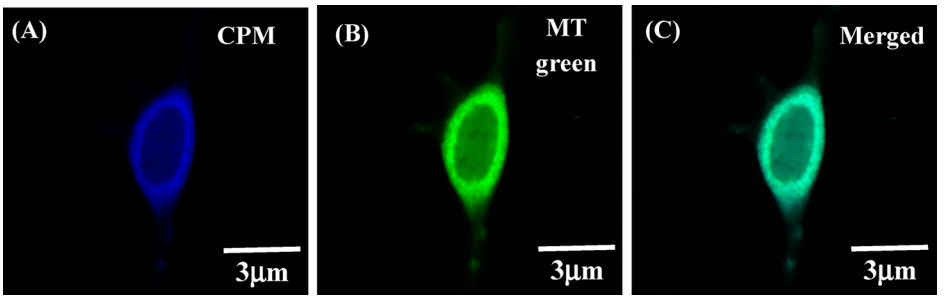

Figure 5. Confocal image of MCF-7: (A) labeled with CPM, (B) labeled with MT-green, and (C) merged image.

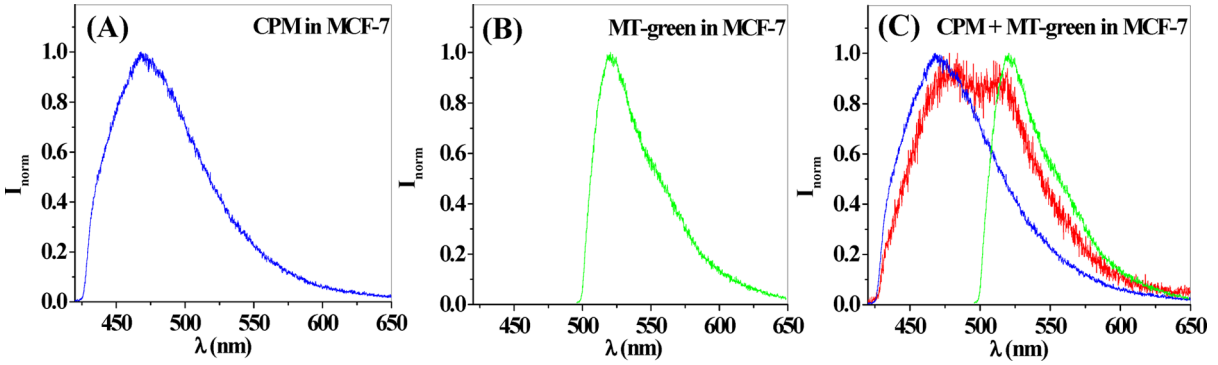

Figure 6. Emission spectra inside a MCF-7: (A) CPM (blue), (B) MT-green (green), and (C) CPM and MT-green both (red).

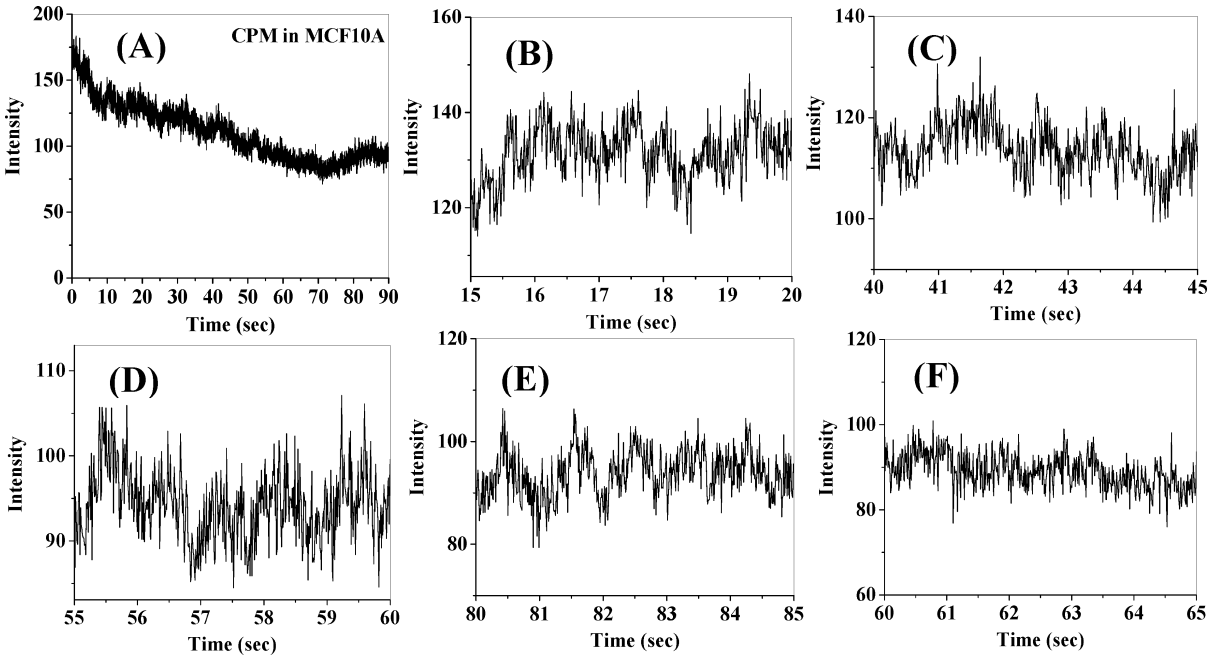

Figure 7. Fluorescence intensity time trajectories. CPM-labeled thiol protein in mitochondria of MCF-10A cell: (A) 0−90, (B) 15−20, (C) 40−45, (D) 55−60, (E) 80−85, and (F) 60−65 s (no oscillation).

To further confirm that CPM resides in the mitochondria, we have performed a colocalization study with a mitochondria selective dye, mitotracker green (MT-green). Figure 2 shows the confocal images of mitochondria in MCF-10A cell labeled by CPM (Figure 2A) and by MT-green (Figure 2B). In Figure 2C, the two figures (Figure 2A,B) are merged. From Figure 2C, it is obvious that the dye CPM colocalizes with MT-green, indicating the presence of both of the dyes in the same region of the cell. Because MT-green resides in mitochondria, we conclude that CPM also localizes in the mitochondria.

Figure 3 shows emission spectra recorded under a confocal microscope of a MCF-10A cell labeled by CPM (Figure 3A), by MT-green (Figure 3B), and by both (Figure 3C). Note that the emission spectra recorded under the microscope correspond to a very small focused region (∼200 nm) of the cell. The emission spectrum in Figure 3C is clearly the sum of the individual emission spectra of CPM and MT-green. From

dx.doi.org/10.1021/jp503808z | J. Phys. Chem. B XXXX, XXX, XXX−XXX

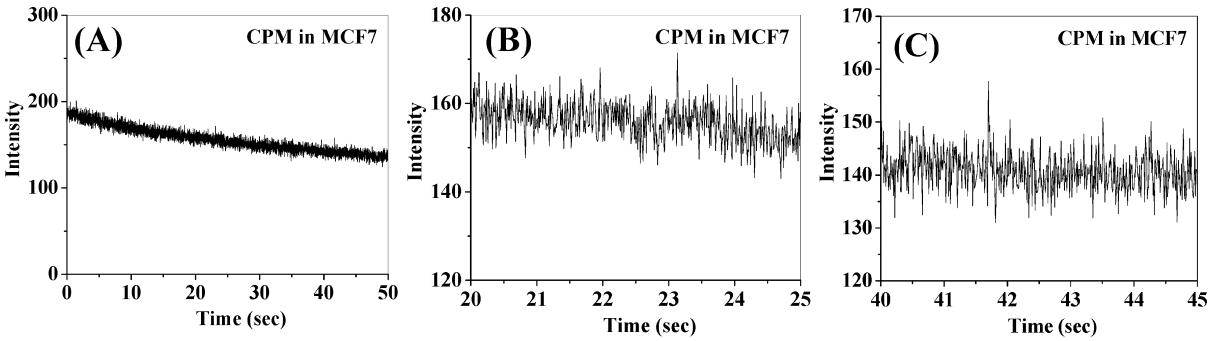

Figure 8. Fluorescence intensity time trajectories. CPM in MCF-7 breast cancer cell: (A) 0−50, (B) 20−25, and (C) 40−45 s.

Figure 3C, it is evident that both CPM and MT-green localize in the same mitochondria probed by the microscope. This further supports the contention that CPM labels the mitochondrial thiol proteins.

3.1.2. Localization of CPM in MCF-7: Clustered Mitochondria in Peri-Nuclear Region. Figure 4 shows the confocal images of a live breast cancer cell MCF-7 stained by CPM. In the case of MCF-7 cell the dye preferentially labels the clustered mitochondria in the peri-nuclear region, as evidenced from the strong fluorescence from the peri-nuclear region.

To confirm that CPM resides in the clustered mitochondria in the peri-nuclear region inside the breast cancer cell MCF-7, we have performed a colocalization study with MT-green. Figure 5 shows the confocal images of MCF-7 cell stained by CPM (Figure 5A) and by MT-green (Figure 5B). In Figure 5C, the two figures (Figure 5A,B) are merged. From Figure 5C, it is obvious that the dye CPM colocalizes with MT-green, indicating the presence of both of the dyes in the peri-nuclear region as clustered mitochondria.[52−58]

Figure 6 gives emission spectra of a MCF-7 cell stained by CPM (Figure 6A), by MT-green (Figure 6B), and by both (Figure 6C). It is readily seen that both CPM and MT-green give emission from the same mitochondrial position in the peri-nuclear region. This further supports the conclusion that CPM labels the thiol proteins in the clustered mitochondria.

3.2. Structural Fluctuations. *3.2.1. CPM in Mitochondria of MCF 10A: Fluorescence Oscillations.* Figure 7 shows intensity versus time trajectories for CPM labeled mitochondrial thiol protein in MCF-10A cell. It is readily seen in Figure 7 that the CPM labeled thiol proteins in the mitochondria display an intermittent oscillation in the fluorescence intensity. As shown in Figure 7 in the 90 s period (0−90 s, Figure 7A) such oscillations were observed for the following periods -15−20 s (Figure 7B), 40−45 s (Figure 7C), 55−60 s (Figure 7D) and 80−85 s (Figure 7E). At other times, the amplitude of oscillation is much less (e.g., 60−65 s in Figure 7F).

3.2.2. CPM in MCF-7: No Fluorescence Oscillations. In sharp contrast with the normal breast cell, the amplitude of oscillation is very much less for breast cancer cell at all time intervals (Figure 8). It may be mentioned that the dye CPM localizes in the clustered mitochondria in the peri-nuclear region of MCF-7 cell instead of discrete mitochondrial thiol proteins in the case of MCF-10A cell. Inside the clustered mitochondria, the red-ox cycle does not occur efficiently.[52−58] This could be the reason for less prominent oscillation in this case.

In summary, the observed oscillation in fluorescence intensity in the mitochondria of MCF-10A is a direct proof of efficient red-ox signaling pathways in the discrete mitochondria.

3.3. Solvation Dynamics of CPM in Mitochondria. Because CPM is a solvation probe and is able to monitor the changes in the microenvironment of the system under consideration, we studied solvation dynamics at the mitochondria of MCF-10A and peri-nuclear region of MCF-7 breast cancer cell.

In both cases the fluorescent transients display decay at blue end (at short emission wavelength) and rise preceding the decay at red end (at long emission wavelength) (Figure 9).

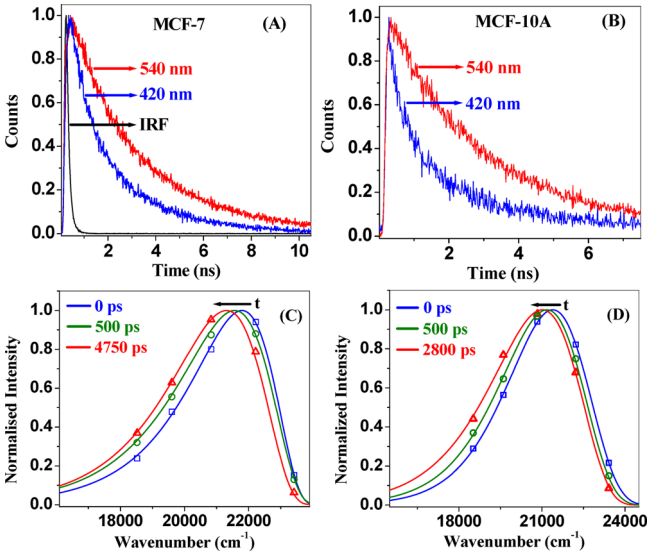

Figure 9. Fluorescence transients at λ_{ex} = 405 nm: (A) CPM in MCF-7 and (B) CPM in MCF-10A. Time-resolved emission spectra, TRES: (C) CPM in MCF-7 and (D) CPM in MCF-10A.

This clearly indicates that solvation dynamics is occurring at the discrete mitochondria (in MCF-10A) as well as in the clustered mitochondria in peri-nuclear region (in MCF-7).

The emission maximum of CPM in the mitochondria of MCF-10A (473 nm) is close to that of CPM-labeled human serum albumin (HSA) in 6 M guanidium hydrochloride (472 nm).[66] The emission maximum of CPM in the mitochondria of MCF-7 (467 nm) resembles that of CPM-labeled HSA in 1.5 M room-temperature ionic liquid (RTIL).[66] Thus, we have assumed the $\upsilon_{em}^{theo}(0)$ of CPM in the mitochondria of MCF-10A and MCF-7 cell to be same as that for of CPM labeled HSA in 6 M guanidium hydrochloride (21 555 cm^{-1})[66] and in 1.5 M RTIL (21 835 cm^{-1}),[66] respectively. As shown in Table 1, 30%

dx.doi.org/10.1021/jp503808z | J. Phys. Chem. B XXXX, XXX, XXX−XXX

Table 1. Parameters of Decay of Correlation Function ($C(t)$) of CPM Attached to the Mitochondrial Thiol Protein in MCF-10A and Perinuclear Region in MCF-7 Cell

system	$\Delta\nu$ [$\nu(0)$] cm^{-1}	τ_1 (a_1) (ps)	τ_2 (a_2) (ps)	$<\tau_s>$ (ps)[a]	% missed
MCF-10A	400 [21 400]	150 (0.25)	1100 (0.75)	850	30
MCF-7	500 [21 800]	350 (0.4)	2100 (0.6)	1400	10

[a]±50 ps.

of solvation dynamics is missed for CPM in MCF-10A cell, while 10% is missed in the case of CPM in MCF-7 cell.

The TRES of CPM inside MCF-7 and MCF-10A (Figure 9C,D) was constructed from the steady-state emission spectra and the fluorescence transients following the procedure by Maroncelli and Fleming.[64] The TRES indicates that the total dynamic Stokes shift (DSS) of CPM inside MCF-7 and MCF-10A is 500 and 400 cm^{-1}, respectively (Table 1). Figure 10

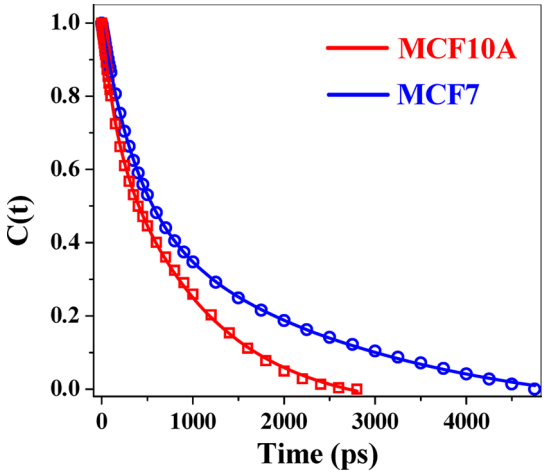

Figure 10. Decay of solvent correlation function, $C(t)$, for CPM in MCF-10A (red) and CPM in MCF-7 (blue).

shows the decay of solvent correlation function ($C(t)$) of CPM bound to the thiol containing proteins in discrete mitochondria in MCF-10A and in the clustered mitochondria in the peri-nuclear region in MCF-7 cell. The decay parameters of $C(t)$ are given in Table 1. The decay of $C(t)$ of CPM labeled mitochondrial thiol protein in MCF-10A displays two components, 150 (25%) and 1100 ps (75%), with an average solvation time ($<\tau_s>$) ≈ 850 ± 50 ps (Table 1). In contrast, decay of $C(t)$ of CPM bound to the peri-nuclear region in MCF-7 displays two components: 350 (40%) and 2100 ps (60%), with an average solvation time ($<\tau_s>$) ≈ 1400 ± 50 ps (Table 1).

4. DISCUSSION

The most important finding of the present work is the intermittent oscillation in fluorescence intensity of CPM in the mitochondria region of MCF-10A cell. This result indicates that oscillation in fluorescence intensity is related to red-ox signaling pathway in the mitochondria.

Using a thiol-reactive maleimide dye (similar to CPM), Liebler and coworkers previously reported that the thiol-containing proteins are associated with cellular oxidative stress and red-ox signaling pathway in the mitochondrial membrane.[47] The GSH/GSSG red-ox cycle occurring in mitochondria gives rise to oscillation in inner mitochondrial membrane potential.[40] These thiol-containing proteins interact with the glutathione pool in the mitochondria during oxidative stress by ROS to form disulfide bonds.[51] The repeated cycles of oxidation−reduction of thiol-containing proteins lead to stabilization and folding of thiol containing proteins in mitochondria. The consequent thiol/disulfide exchange (Scheme 1) gives rise to reversible, intermittent changes in the structure of the mitochondrial membrane protein and microenvironment of CPM. This causes fluctuation in fluorescence intensity of CPM covalently bound to the mitochondrial thiol protein in MCF-10A.

It is evident that the amplitude of structural oscillation in the case of the cancer cell (MCF-7) is much less than that in the normal cell (MCF-10A). This difference may be due to the difference in efficiencies of red-ox cycle in the cancer cell (clustered mitochondria in the peri-nuclear region) and that in the normal cell (discrete mitochondria).[52−58]

We now determine the time periods of oscillations in the case of MCF-10A. For this, we have used fast Fourier transform (FFT) filter (Figure 11A,B). As shown in Figure 11B, the period of oscillation is not constant and the half-period varies in the range 0.5 to 1.3 s (for various peaks in one bunch of oscillation and for different bunches in different sets). However, the majority of such oscillations exhibit half-period ∼1 s. In

Scheme 1. Thiol−Disulfide Exchange in Mitochondria

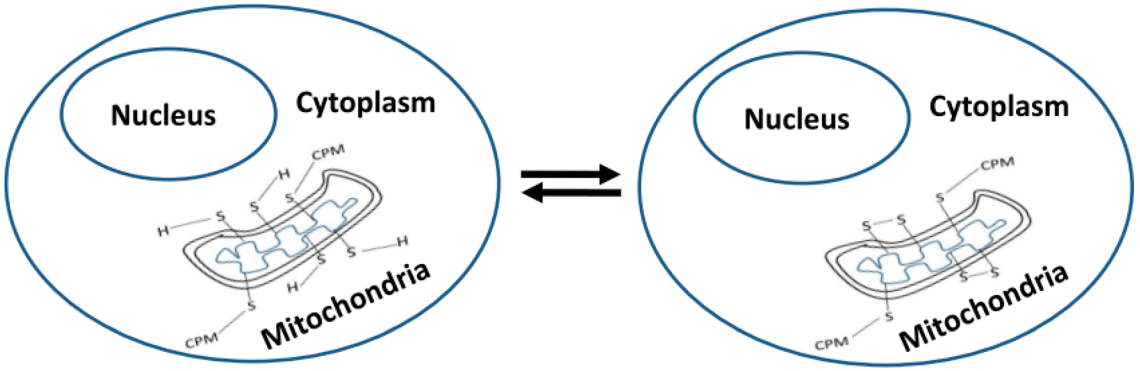

dx.doi.org/10.1021/jp503808z | J. Phys. Chem. B XXXX, XXX, XXX−XXX

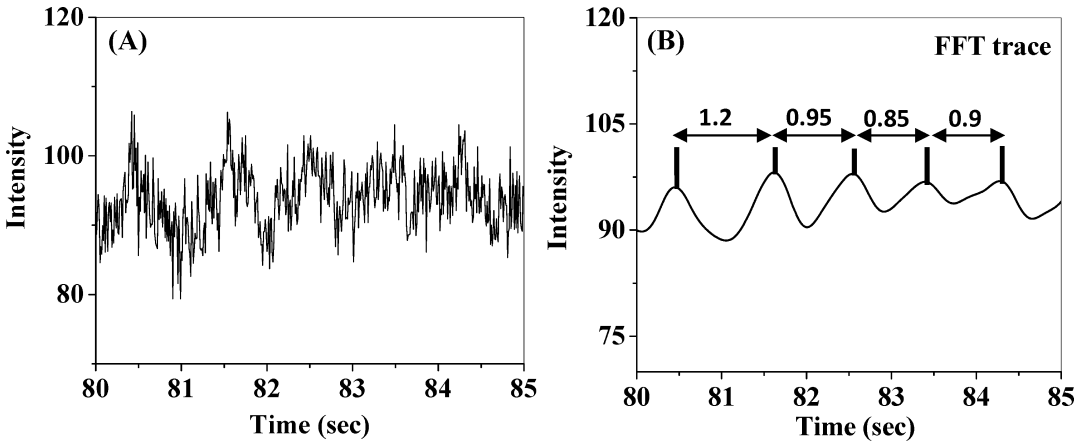

Figure 11. Fluorescence intensity versus time trajectories: CPM-labeled mitochondrial thiol protein in MCF-10A cell: (A) 80−85 s and (B) 80−85 s smoothed by FFT (showing half periods).

summary, the time trace indicates that the fluorescence intensity oscillates intermittently with a varying time period separated by certain silent ("quiescent") periods, in which there is no oscillation. It further indicates that intermittent structural oscillation is not peculiar to cell membrane region (as previously reported[38]) but can also occur in other regions of a cell (e.g., mitochondria), which participates in red-ox signaling. It may be mentioned that such intermittent oscillations in fluorescence intensity were previously observed by Lu and coworkers[19] for an enzyme (HPPK). They ascribed these oscillations due to the conformational transition between different active states.

It may be noted that for many different kinds of cell the oscillation in membrane potential occurs on a time scale ranging from a few seconds to milliseconds.[33−35] In our case, the observed oscillation of fluorescence intensity of CPM bound to mitochondrial thiol proteins in MCF-10A echoed well with the dynamical structure of mitochondria.

We will now infer the polarity of the microenvironment of CPM in two different breast cell MCF-10A and MCF-7 from the emission maxima. The steady-state emission maximum of CPM bound to thiol protein is a good indicator of local polarity of the microenvironment. The emission maxima of CPM-bound mitochondrial thiol protein ($\lambda_{em} \approx 473$ nm, Figure 12) in MCF-10A is red-shifted by 13 nm compared with CPM-labeled HSA protein ($\lambda_{em} \approx 460$ nm) in pH ~7 buffer.[66] This suggests that microenvironment of CPM at the mitochondria of MCF-10A is more polar and exposed than that inside HSA. In contrast, the emission maxima of CPM in peri-nuclear region of breast cancer cell MCF-7 are blue-shifted by 6 nm ($\lambda_{em} \approx 467$ nm, Figure 12) compared with normal breast cell MCF-10A. Note that in the MCF-7 cell mitochondria are clustered in the peri-nuclear region. Because of clustering the microenvironment of CPM is more hydrophobic in MCF-7 than that in the discrete mitochondria in MCF-10A. This results in lower local polarity in the mitochondria of MCF-7 compared with that in MCF-10A. In both cases (MCF-7 and MCF-10A), the emission maxima of CPM are blue-shifted compared with CPM at the membrane of CHO cell ($\lambda_{em} \approx 476$ nm).[38] This is because at the cell membrane CPM experiences an environment highly exposed to the extracellular region, compared with intracellular organelles (mitochondria and peri-nuclear region) in MCF-10A and MCF-7 cell.

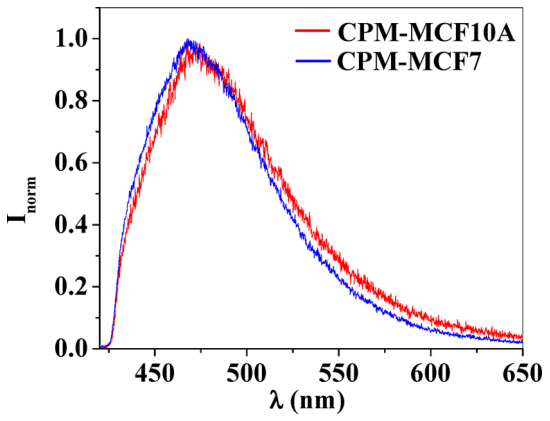

Figure 12. Emission spectra of CPM in mitochondria of normal breast cell MCF-10A (red) and peri-nuclear region of MCF-7 breast cancer cell (blue).

Finally, we discuss solvation dynamics of CPM in mitochondria of normal breast cell MCF-10A and peri-nuclear region of breast cancer cell, MCF-7. Solvation dynamics[1−15] controls dynamics of polar reactions. The average solvation time ($<\tau_s>$) in MCF-10A and MCF-7 cell is 850 and 1400 ps, respectively. Thus, the average solvation time in peri-nuclear region of breast cancer cell is approximately two times slower than the solvation time in mitochondria of normal breast cell. As previously mentioned, in MCF-7 cell, the mitochondria are clustered in nature. Thus, the thiol groups in the proteins present in these clustered mitochondria will be less exposed to the solvent (water present in the mitochondrial matrix). This is reflected in approximately two times slower solvation in the case of MCF-7, compared with MCF-10A. In addition, the average solvation time in both the cases is substantially slower compared with that (1 ps) in the bulk water. In this regard, it may be mentioned that inside mitochondria different kinds of biochemical reactions are going on including metabolism, proton transfer, electron transport reaction, crabs cycle, oxidation−reduction, and different ion-channels signaling.[39−58] Thus, the observed slow dynamics of the water bound to mitochondrial thiol proteins may play a crucial role in controlling the efflux of ions through ion channels and transport as well as metabolism of different biomolecules in mitochondria.

dx.doi.org/10.1021/jp503808z | J. Phys. Chem. B XXXX, XXX, XXX−XXX

It may be mentioned that both the solvation time in the case of normal breast cell MCF-10A and breast cancer cell MCF-7 are slower compared with that ($<\tau_s>$ = 475 ps)[38] at the membrane region in the CHO cell. This is because at the cell membrane, CPM is covalently bound to the exofacial thiol groups and hence assumes an environment highly exposed to the extracellular region. On the contrary, mitochondria are intracellular organelles and hence exhibit relatively slower solvation dynamics than that at the cell membrane.

5. CONCLUSIONS

This work reveals for the first time structural oscillations and solvation dynamics of mitochondria of a live cell. The covalent binding of the probe ensures precise information with high spatial resolution. It is demonstrated that the structural oscillations depend on the efficiency of red-ox cycle. In the discrete mitochondria of the normal human breast cell, MCF-10A where red-ox is efficient, a prominent intermittent oscillation in the fluorescence intensity of the probe is observed because of the fluctuation in the local polarity. In the case of breast cancer cell (MCF-7), the inefficient red-ox process reduces magnitude of intermittent structural fluctuation. The local polarity in the two mitochondria is found to be lower than that at the highly exposed membrane region of CHO cell. The solvation dynamics in the mitochondria region of both the cell (MCF-10A and MCF-7) is slower compared with the membrane region in CHO cell. The slower solvation dynamics may have an impact on the different kinds of biochemical reactions occurring in mitochondria. Systematic investigation of the structural oscillation and solvation dynamics in different organelles in a live cell may shed new light on cellular biochemical processes.

AUTHOR INFORMATION

Corresponding Authors

*S.S.J.: E-mail: bcssj@iacs.res.in. Fax: (91)-33-2473-2805.
*K.B: E-mail: pckb@iacs.res.in.

Notes

The authors declare no competing financial interest.

ACKNOWLEDGMENTS

We thank the Department of Science and Technology, India for IRHPA Project entitled "*Center for Ultrafast Spectroscopy and Microscopy*" (Project No. IR/S1/CU 02/2009), Council for Scientific and Industrial Research (CSIR), and J. C. Bose Fellowship for generous research support. S.C., R.C., and S.K.D. thank CSIR for awarding fellowships.

REFERENCES

(1) Ingrosso, F.; Ladanyi, B. M. Intermolecular Structure and Collective Dynamics of Supercritical Fluoroform Studied by Molecular Dynamics Simulations. *J. Phys. Chem. B* **2013**, *117*, 654−667.

(2) Pieniazek, P. A.; Lin, Y. S.; Chowdhury, J.; Ladanyi, B. M.; Skinner, J. L. Vibrational Spectroscopy and Dynamics of Water Confined inside Reverse Micelles. *J. Phys. Chem. B* **2009**, *113*, 15017−15028.

(3) Milischuk, A. A.; Krewald, V.; Ladanyi, B. M. Water Dynamics in Silica Nanopores: The self-intermediate scattering functions. *J. Chem. Phys.* **2012**, *136*, 224704−1−10.

(4) Bagchi, B.; Jana, B. Solvation Dynamics in Dipolar Liquids. *Chem. Soc. Rev.* **2010**, *39*, 1936−1954.

(5) Jana, B.; Pal, S.; Bagchi, B. Hydrogen Bond Breaking Mechanism and Water Reorientational Dynamics in the Hydration Layer of Lysozyme. *J. Phys. Chem. B* **2008**, *112*, 9112−9117.

(6) Zhang, Z.; Berkowitz, M. L. Orientational Dynamics of Water in Phospholipid Bilayers with Different Hydration Levels. *J. Phys. Chem. B* **2009**, *113*, 7676−7680.

(7) Pal, S. K.; Peon, J.; Bagchi, B.; Zewail, A. H. Biological Water: Femtosecond Dynamics of Macromolecular Hydration. *J. Phys. Chem. B* **2002**, *106*, 12376−12395.

(8) Bhattacharyya, K.; Bagchi, B. Slow Dynamics of Constrained Water in Complex Geometries. *J. Phys. Chem. A* **2000**, *104*, 10603−10613.

(9) Bhattacharyya, K. Nature of Biological Water: A Femtosecond Study. *Chem. Commun.* **2008**, 2848−2857.

(10) Zhong, D.; Pal, S. K.; Zewail, A. H. Biological Water: A Critique. *Chem. Phys. Lett.* **2011**, *503*, 1−11.

(11) Jha, A.; Ishii, K.; Udgaonkar, J. B.; Tahara, T.; Krishnamoorthy, G. Exploration of the Correlation between Solvation Dynamics and Internal Dynamics of a Protein. *Biochemistry* **2011**, *50*, 397−408.

(12) Andreatta, D.; PérezLustres, J. L.; Kovalenko, S. A.; Ernsting, N. P.; Murphy, C. J.; Coleman, R. S.; Berg, M. A. Power-Law Solvation Dynamics in DNA over Six Decades in Time. *J. Am. Chem. Soc.* **2005**, *127*, 7270−7271.

(13) Sen, S.; Andreatta, D.; Ponomarev, S. Y.; Beveridge, D. L.; Berg, M. A. Dynamics of Water and Ions Near DNA: Comparison of Simulation to Time-Resolved Stokes-Shift Experiments. *J. Am. Chem. Soc.* **2009**, *131*, 1724−1735.

(14) Pal, N.; Verma, S. D.; Sen, S. Probe Position Dependence of DNA Dynamics: Comparison of the Time-Resolved Stokes Shift of Groove-Bound to Base-Stacked Probes. *J. Am. Chem. Soc.* **2010**, *132*, 9277−9279.

(15) Zhang, L.; Kao, Y. T.; Qiu, W.; Wang, L.; Zhong, D. Femtosecond Studies of Tryptophan Fluorescence Dynamics in Proteins: Local Solvation and Electronic Quenching. *J. Phys. Chem. B* **2006**, *110*, 18097−18103.

(16) Elf, J.; Li, G. W.; Xie, X. S. Probing Transcription Factor Dynamics at the Single-Molecule Level in a Living Cell. *Science* **2007**, *316*, 1191−1200.

(17) Blainey, P. C.; van Oijen, A. M.; Banerjee, A.; Verdine, G. L.; Xie, S. X. A Base-excision DNA-repair Protein Finds Intrahelical Lesion Bases by Fast Sliding in Contact with DNA. *Proc. Natl. Acad. Sci. U.S.A.* **2006**, *133*, 5752−5757.

(18) Bagchi, B.; Blainey, P. C.; Xie, X. S. Diffusion Constant of a Nonspecifically Bound Protein Undergoing Curvilinear Motion along DNA. *J. Phys. Chem. B* **2008**, *112*, 6282−6284.

(19) He, Y.; Li, Y.; Mukherjee, S.; Wu, Y.; Yan, H.; Lu, H. P. Probing Single-Molecule Enzyme Active-Site Conformational State Intermittent Coherence. *J. Am. Chem. Soc.* **2011**, *133*, 14389−14395.

(20) Chen, Y.; Hu, D.; Vorpagel, E. R.; Lu, H. P. Probing Single-Molecule T4 Lysozyme Conformational Dynamics by Intramolecular Fluorescence Energy Transfer. *J. Phys. Chem. B* **2003**, *107*, 7947−7956.

(21) Hu, D.; Lu, H. P. Single Molecule Implanting of T4 Lysozyme on Bacterial Cell Surface: Towards Study Single Molecule Enzymatic Reaction in Living Cells. *Biophys. J.* **2004**, *87*, 656−661.

(22) Harms, G. S.; Orr, G.; Montal, M.; Thrall, B. D.; Colson, S. D.; Lu, H. P. Probing Conformational Changes of Gramicidin Ion Channels by Single-Molecule Patch-Clamp Fluorescence Microscopy. *Biophys. J.* **2003**, *85*, 1826−1838.

(23) Chattoraj, S.; Saha, S.; Jana, S. S.; Bhattacharyya, K. Dynamics of Gene Silencing in a Live Cell: Stochastic Resonance. *J. Phys. Chem. Lett.* **2014**, *5*, 1012−1016.

(24) Cai, D.; Hoppe, A. D.; Swanson, J. A.; Verhey, K. J. Kinesin-1 Structural Organization and Conformational Changes Revealed by FRET Stoichiometry in Live Cells. *J. Cell Biol.* **2007**, *176*, 51−63.

(25) Verbrugge, S.; Lechner, B.; Woehlke, G.; Peterman, E. J. Alternating-site Mechanism of Kinesin-1 Characterized by Single-molecule FRET using Fluorescent ATP Analogues. *Biophys. J.* **2009**, *97*, 173−182.

(26) Verbrugge, S.; Lansky, Z.; Peterman, E. J. Kinesin's Step Dissected with Single-motor FRET. *Proc. Natl. Acad. Sci. U.S.A.* **2009**, *106*, 17741−17746.
(27) Maurer, S. P.; Fourniol, F. J.; Bohner, G.; Moores, C. A.; Surrey, T. EBs Recognize a Nucleotide-Dependent Structural Cap at Growing Microtubule Ends. *Cell* **2012**, *149*, 371−382.
(28) Maurer, S. P.; Bieling, P.; Cope, J.; Hoenger, A.; Surrey, T. GTPγS Microtubules Mimic the Growing Microtubule End Structure Recognized by End-Binding Proteins (EBs). *Proc. Natl. Acad. Sci. U.S.A.* **2011**, *108*, 3988−3993.
(29) Aon, M. A.; Roussel, M. R.; Cortassa, S.; Rourke, B. O.; Murray, D. B.; Beckmann, M.; Lloyd, D. The Scale-Free Dynamics of Eukaryotic Cells. *PLoS One* **2008**, *3*, e3624-1−e3624-12.
(30) Longtin, A.; Bulsara, A.; Moss, F. Time-Interval Sequences in Bistable Systems and the Noise-Induced Transmission of Information by Sensory Neurons. *Phys. Rev. Lett.* **1991**, *67*, 656−659.
(31) Domke, J.; Parak, W. J.; George, M.; Gaub, H. E.; Radmacher, M. Mapping the Mechanical Pulse of Single Cardiomyocytes with the Atomic Force Microscope. *Eur. Biophys. J.* **1999**, *28*, 179−186.
(32) Maksym, G. N.; Fabry, B.; Butler, J. P.; Navajas, D.; Tschumperlin, D. J.; Laporte, J. D.; Fredberg, J. J. Mechanical Properties of Cultured Human Airway Smooth Muscle Cells from 0.05 to 0.4 Hz. *J. Appl. Physiol.* **2000**, *89*, 1619−1632.
(33) Domnisoru, C.; Kinkhabwala, A. A.; Tank, D. W. Membrane Potential Dynamics of Grid Cells. *Nature* **2013**, *495*, 199−204.
(34) Chapman, C. A.; Lacaille, J. C. Intrinsic Theta-Frequency Membrane Potential Oscillations in Hippocampal CA1 Interneurons of Stratum Lacunosum-Moleculare. *J. Neurophysiol.* **1999**, *81*, 1296−1307.
(35) Atwater, I.; Dawson, C. M.; Scott, A.; Eddlestone, G.; Rojas, E. The Nature of the Oscillatory Behavior in Electrical Activity for Pancreatic β-Cell. In *Biochemistry Biophysics of the Pancreatic-β-Cell*; Georg Thieme Verlag: New York, 1980; pp 100−107.
(36) Olsen, L. F.; Andersen, A. Z.; Lunding, A.; Brasen, J. C.; Poulsen, A. K. Regulation of Glycolytic Oscillations by Mitochondrial and Plasma Membrane H^+-ATPases. *Biophys. J.* **2009**, *96*, 3850−3861.
(37) Torres, A. G.; Gait, M. J. Exploiting Cell Surface Thiols to Enhance Cellular Uptake. *Trends Biotechnol.* **2012**, *30*, 185−190.
(38) Ghosh, S.; Chattoraj, S.; Bhattacharyya, K. Solvation Dynamics and Intermittent Oscillation of Cell Membrane: Live Chinese Hamster Ovary Cell. *J. Phys. Chem. B* **2014**, *118*, 2949−2956.
(39) Friedman, J. R.; Nunnari, J. Mitochondrial Form and Function. *Nature* **2014**, *505*, 335−343.
(40) Aon, M. A.; Cortassa, S.; Maack, C.; Rourke, B. O. Sequential Opening of Mitochondrial Ion Channels as a Function of Glutathione Redox Thiol Status. *J. Biol. Chem.* **2007**, *282*, 21889−21900.
(41) Sevier, C. S.; Kaiser, C. A. Formation and Transfer of Disulphide Bonds in Living Cells. *Nat. Rev. Molecular Cell Biol.* **2002**, *3*, 836−847.
(42) Collins, Y.; Chouchani, E. T.; James, A. M.; Menger, K. E.; Cochemé, H. M.; Murphy, M. P. Mitochondrial Redox Signaling at a Glance. *J. Cell Sci.* **2012**, *125*, 801−806.
(43) Aon, M. A.; Cortassa, S.; Rourke, B. O. The Fundamental Organization of Cardiac Mitochondria as a Network of Coupled Oscillators. *Biophys. J.* **2006**, *91*, 4317−4327.
(44) Lin, T. K.; Hughes, G.; Muratovska, A.; Blaikie, F. H.; Brookes, P. S.; Usmar, V. D.; Smith, R. A. J.; Murphy, M. P. Specific Modification of Mitochondrial Protein Thiols in Response to Oxidative Stress. *J. Biol. Chem.* **2002**, *277*, 17048−17056.
(45) James, A. M.; Collins, Y.; Logan, A.; Murphy, M. P. Mitochondrial Oxidative Stress and The metabolic syndrome. *Trends Endocrinol. Metab.* **2012**, *23*, 429−434.
(46) Hurd, T. R.; Filipovska, A.; Costa, N. J.; Dahm, C. C.; Murphy, M. P. Disulphide Formation on Mitochondrial Protein Thiols. *Biochem. Soc. Trans.* **2005**, *33*, 1390−1393.
(47) Wong, H. L.; Liebler, D. C. Mitochondrial Protein Targets of Thiol-Reactive Electrophiles. *Chem. Res. Toxicol.* **2008**, *21*, 796−804.
(48) Aon, M. A.; Cortassa, S.; Rourke, B. O. Mitochondrial Oscillations in Physiology and Pathophysiology. *Adv. Exp. Med. Biol.* **2008**, *641*, 98−117.
(49) Kurz, F. T.; Aon, M. A.; Rourke, B. O.; Armoundas, A. A. Spatio-temporal Oscillations of Individual Mitochondria in Cardiac Myocytes Reveal Modulation of Synchronized Mitochondrial Clusters. *Proc. Natl. Acad. Sci. U. S. A.* **2010**, *107*, 14315−14320.
(50) Griffiths, E. J.; Rutter, G. A.; Griffiths, E. J.; Rutter, G. A. Mitochondrial Calcium as a Key Regulator of Mitochondrial ATP Production in Mammalian Cells. *Biochim. Biophys. Acta* **2009**, *1787*, 1324−1333.
(51) Cortassa, S.; Aon, M. A.; Winslow, R. L.; Rourke, B. O. A Mitochondrial Oscillator Dependent on Reactive Oxygen Species. *Biophys. J.* **2004**, *87*, 2060−2073.
(52) Al-Mehdi, A. B.; Pastukh, V. M.; Swiger, B. M.; Reed, D. J.; Patel, M. R.; Bardwell, G. C.; Pastukh, V. V.; Alexeyev, M. F.; Gillespie, M. N. Peri-nuclear Mitochondrial Clustering Creates an Oxidant-Rich Nuclear Domain Required for Hypoxia-Induced Transcription. *Sci. Signal.* **2012**, *5*, ra47.
(53) Hamacher-Brady, A.; Stein, H. A.; Turschner, S.; Toegel, I.; Mora, R.; Jennewein, N.; Efferth, T.; Eils, R.; Brady, N. R. Artesunate Activates Mitochondrial Apoptosis in Breast Cancer Cells via Iron-catalyzed Lysosomal Reactive Oxygen Species Production. *J. Biol. Chem.* **2011**, *286*, 6587−6601.
(54) Esposti, M. D.; Hatzinisiriou, I.; McLennan, H.; Ralph, S. Bcl-2 and Mitochondrial Oxygen Radicals. *J. Biol. Chem.* **1999**, *274*, 29831−29837.
(55) Vives-Bauza, C.; Zhou, C.; Huang, Y.; Cui, M.; de Vries, R. L. A.; Kim, J.; May, J.; Tocilescu, M. A.; Liu, W.; Ko, H. S.; Magrané, J.; Moore, D. J.; Dawson, V. L.; Grailhe, R.; Dawson, T. M.; Li, C.; Tieu, K.; Przedborski, S. PINK1-dependent Recruitment of Park into Mitochondria in Mitophagy. *Proc. Natl. Acad. Sci. U. S. A.* **2010**, *107*, 378−383.
(56) Yee, K. S.; Wilkinson, S.; James, J.; Ryan, K. M.; Vousden, K. H. PUMA- and Bax-Induced Autophagy Contributes to Apoptosis. *Cell Death Differ.* **2009**, *16*, 1135−1145.
(57) Wu, L.; Li, Z.; Zhang, Y.; Zhang, P.; Zhu, X.; Huang, J.; Ma, T.; Lu, T.; Song, Q.; Li, Q.; Guo, Y.; Tang, J.; Ma, D.; Chen, K. H.; Qiu, X. Adenovirus-expressed Human Hyperplasia Suppressor Gene Induces Apoptosis in Cancer Cells. *Mol. Cancer Ther.* **2008**, *7*, 222−232.
(58) Thomas, W. D.; Zhang, X. D.; Franco, A. V.; Nguyen, T.; Hersey, P. TNF-Related Apoptosis-Inducing Ligand-Induced Apoptosis of Melanoma Is Associated with Changes in Mitochondrial Membrane Potential and Peri-nuclear Clustering of Mitochondria. *J. Immunol.* **2000**, *165*, 5612−5620.
(59) Chowdhury, R.; Chattoraj, S.; Sen Mojumdar, S.; Bhattacharyya, K. FRET between a Donor and an Acceptor Covalently Bound to Human Serum Albumin in Native and Non-native states. *Phys. Chem. Chem. Phys.* **2013**, *15*, 16286−16293.
(60) Chowdhury, R.; Jana, B.; Saha, A.; Ghosh, S.; Bhattacharyya, K. Confocal Microscopy of Cytoplasmic Lipid Droplets in a Live Cancer Cell: Number, Polarity, Diffusion and Solvation Dynamics. *Med. Chem. Commun.* **2014**, *5*, 536−539.
(61) Hess, S. T.; Sheets, E. D.; Wagenknecht-Wiesner, A.; Heikal-Simultaneous, A. A. Quantitative Analysis of the Fluorescence Properties of Intrinsically Fluorescent Proteins in Living Cells. *Biophys. J.* **2003**, *85*, 2566−2580.
(62) Fisz, J. J. Fluorescence Polarization Spectroscopy at Combined High-Aperture Excitation and Detection: Application to One-Photon-Excitation Fluorescence Microscopy. *J. Phys. Chem. A* **2007**, *111*, 8606−8621.
(63) Petrasek, Z.; Schwille, P. Precise Measurement of Diffusion Coefficients using Scanning Fluorescence Correlation Spectroscopy. *Biophys. J.* **2008**, *94*, 1437−1448.
(64) Maroncelli, M.; Fleming, G. R. Picosecond Solvation Dynamics of Coumarin 153: The Importance of Molecular Aspects of Solvation. *J. Chem. Phys.* **1987**, *86*, 6221−6239.

(65) Fee, R. S.; Maroncelli, M. Estimating the Time-zero Spectrum in Time-resolved Emission Measurements of Solvation Dynamics. *Chem. Phys.* **1994**, *183*, 235−247.
(66) Chowdhury, R.; Sen Mojumdar, S.; Chattoraj, S.; Bhattacharyya, K. Effect of Ionic Liquid on the Native and Denatured State of a Protein Covalently Attached to a Probe: Solvation Dynamics Study. *J. Chem. Phys.* **2012**, *137*, 055104-1−055104-8.